J Mater Sci (2009) 44:3687–3693
DOI 10.1007/s10853-009-3493-9

Spindlelike Y_2O_3:Eu^{3+} nanorod bundles: hydrothermal synthesis and photoluminescence properties

Shengliang Zhong · Shijin Wang · Huaping Xu · Haoqing Hou · Zubiao Wen · Ping Li · Shangping Wang · Rong Xu

Received: 8 January 2009 / Accepted: 13 April 2009 / Published online: 7 May 2009

Abstract Uniform spindlelike $Y(OH)_3$ nanorod bundles were successfully prepared for the first time via a simple hydrothermal method at 200 °C for 12 h with the presence of $Na_2H_2EDTA \cdot 2H_2O$ (EDTA). Scanning electron microscope (SEM) images show that the obtained $Y(OH)_3$ spindlelike nanorod bundles have a length of about 11 μm and a diameter of about 2 μm in the middle part. The nanorod bundles are composed of numerous nanorods, and all these nanorods are orientationally aligned and grow uniformly along the bundles. The individual nanorod is with typical width of about 100 nm, thickness of about 40 nm, and length longer than 1 μm. The effects of reaction temperature, reaction time, and the concentration of NaOH and EDTA on the sizes and morphologies of the products have been investigated. The possible formation mechanism of the nanorod bundles was suggested. Spindlelike Y_2O_3 nanorod bundles were obtained after thermal treatment of the as-obtained $Y(OH)_3$ nanorod bundles at 700 °C for 4 h. X-ray powder diffraction (XRD) results demonstrate that the as-prepared $Y(OH)_3$ and Y_2O_3 are attributed to hexagonal phase and cubic phase, respectively. Eu^{3+} doped Y_2O_3 nanorod bundles were also prepared and their photoluminescence (PL) properties were investigated.

S. Zhong (✉) · S. Wang · H. Hou · Z. Wen · P. Li · S. Wang · R. Xu
College of Chemistry and Chemical Engineering, Jiangxi Normal University, Nanchang 330022, People's Republic of China
e-mail: zslxhx@yahoo.com.cn

H. Xu
Gannan Medical University, Ganzhou 341000, People's Republic of China

Introduction

Rare earth oxides find wide range applications in catalysis, optics, biological labeling, magnetism, etc. [1–3]. Among them, Y_2O_3 has been intensively studied owing to its chemical and physical properties, such as high permittivity, high melting point, a relatively large band gap energy, etc. It is a widely used engineering material, such as optics, advanced ceramics [4, 5], superconductor, sensor [6, 7], and insulator materials [8]. For example, Y_2O_3:Eu^{3+} is widely used in fluorescent lights and cathode ray tube owing to its high luminescence quantum efficiency [9]. Moreover, it is a promising phosphor material being developed for field emission display devices [10].

As is well known, the properties of the products depend greatly on the morphologies and structures of the materials. More applications of Y_2O_3 may emerge if shape-controlled nanostructures could be achieved with high complexity. Much attention has been paid to the morphology control of Y_2O_3 in recent years. Untill now, Y_2O_3 nanostructures, such as nanotube [11–13], nanowire [14–16], nanorod [15–18], nanobelt [19, 20], and nanodisk [21], microprisms with trilobal cross section [22] and nestlike structures [23] have been reported. To the best of our knowledge, spindlelike Y_2O_3 has not been reported. And there are few reports on the management of Y_2O_3 nanophase. In this work, spindlelike yttrium hydroxide nanorod bundles composed of numerous nanorods were fabricated via a facile hydrothermal method. Y_2O_3 spindlelike nanorod bundles were obtained by thermal decomposition of the $Y(OH)_3$ precursor at 700 °C for 4 h. Spindlelike Y_2O_3:Eu^{3+} nanorod bundles were also fabricated for the first time and their photoluminescence properties were studied. The products are characterized by XRD, SEM, and fluorescence spectrometer.

Experimental section

Synthesis

All the chemical reagents used were of analytical grade and used as received without further purification. In a typical Experiment, 0.64 mmol $Y(NO_3)_3 \cdot 6H_2O$ was dissolved in 28.8 mL deionized water under stirring. Then 0.64 mmol EDTA was added to the $Y(NO_3)_3$ solution. After stirring for 30 min, 3.2 mL NaOH (10 M) was added to the above solution. After being stirred for another 30 min, the mixture was transferred into a 42 mL Teflon-lined stainless steel autoclave and then was sealed and got heated at 200 °C for 12 h. After being cooled to room temperature naturally, the white precipitates were centrifuged and washed with alcohol and deionized water for several times. Finally, the product was dried at 80 °C for 6 h in air. The Y_2O_3 nanorod bundles were obtained by thermal treatment of the corresponding $Y(OH)_3$ nanorod bundles at 700 °C for 4 h in the air. The preparation of Y_2O_3:Eu^{3+}(5%) nanorod bundles is similar to above procedure, just replacing five molar % of $Y(NO_3)_3 \cdot 6H_2O$ with $Eu(NO_3)_3 \cdot 6H_2O$.

Characterization

The phase purity and crystalline phase of the products were characterized on a Philips X' Pert Pro Super X-ray diffractometer equipped with graphite monochromatized Cu Kα radiation ($\lambda = 1.541\ 78$ Å). The morphology and size of the samples were examined by a field-emission scanning electron microanalyzer (JEOL JSM-6700F, 15 kV) and an environmental scanning electron microanalyzer (QUANTA 200). The PL properties were examined on a Fluorolog3-TAU-P fluorescence spectrometer at room temperature.

Results and discussion

Table 1 lists the detailed experimental conditions of the as-prepared products. The effects of reaction time, reaction temperature, concentrations of EDTA, and sodium hydroxide on the synthesis were studied.

Typical SEM images and XRD patterns of the products

Figure 1 displays the XRD patterns of the as-prepared $Y(OH)_3$ products prepared at different reaction temperature and Y_2O_3 obtained after thermal treatment of sample 1 at 700 °C for 4 h. All the peaks of the XRD pattern in Fig. 1a, b, c can be indexed as pure hexagonal phase of $Y(OH)_3$ (Joint Committee for Powder Diffraction Studies (JCPDS) card No. 83-2042). It can be seen from the patterns that the crystallinity of the sample prepared at 160 °C (Fig. 1b) is much higher than that of the product prepared at 80 °C (Fig. 1a). While the crystallinity of the product prepared at 200 °C (Fig. 1c) is only slightly higher than that of the product prepared at 80 °C. From which it becomes obvious that the crystallinity of the product increases with increase of reaction temperature. The crystallite size of the samples is estimated by the Scherrer equation. By using the strongest peak (100) at $2\theta = 16.229°$, the average size of the $Y(OH)_3$ nanorods of the products prepared at 80, 160, and 200 °C is calculated to be about 25, 31, and 38 nm, respectively. It is clear that the diameters of the nanorods increase with the increase of reaction temperature, which is in accordance with the crystallinity of the products. The XRD pattern of the product prepared after annealing sample 1 at 700 °C in the air for 4 h is shown in Fig. 1d. As can be seen, all peaks are in good agreement with cubic Y_2O_3 (JCPDS card No. 86-1107). The average size of the product obtained after calcinations at 700 °C for 4 h is about 34 nm, which is a bit smaller than that of the corresponding $Y(OH)_3$ nanorods.

The morphology and structure of the as-synthesized $Y(OH)_3$ and Y_2O_3 powder were further investigated by SEM. As shown in Fig. 2a, the overall morphology of the sample 1 indicates that there exist a great deal of uniform spindlelike structures in high yield. The microspindles are in the length of about 11 μm and diameter about 2 μm in the middle part. Typical nanorod bundles (Fig. 2b) reveal that the nanorod bundles are built from $Y(OH)_3$ nanorods with typical widths of about 100 nm, thicknesses of about 40 nm, and lengths longer than 1 μm. The thickness of the nanorod is similar with the value calculated from the XRD pattern. Furthermore, the individual nanorods are straight and smooth and the nanorods are tightly bound together. All the nanorods are orientationally aligned, and they grow uniformly along the bundles. Moreover, these nanorod bundles are very dispersive and size distribution is also very uniform. Spindlelike Y_2O_3 nanorod bundles were obtained from the spindlelike $Y(OH)_3$ nanorod bundles by calcinations of sample 1 at 700 °C for 4 h. The general morphology of the as-prepared Y_2O_3 samples is clearly shown in Fig. 2c. Careful observation (Fig. 2d) shows that the Y_2O_3 nanostructures consist of nanorods in a parallel assembly. It is interesting that both Y_2O_3 and its precursor almost possess the same morphology, even such a transformation has chemical process.

Effect of reaction time

To understand the formation process of the spindlelike nanorod bundles, time-dependent experiments were carried out at different reaction stage. When the reaction time is 1 h, the products are mainly microspindles and many nanoparticles with a size smaller than 100 nm are also

Table 1 Product obtained under different hydrothermal conditions

Sample	Temperature/°C	Time/h	$[Y(NO_3)_3]$/mol L^{-1}	[EDTA]/mol L^{-1}	[NaOH]/mol L^{-1}
1	200	12	0.02	0.02	1
2	200	1	0.02	0.02	1
3	200	6	0.02	0.02	1
4	200	12	0.02	0.04	1
5	200	12	0.02	0.10	1
6	200	12	0.02	0.02	3
7	200	12	0.02	0.02	5
8	80	12	0.02	0.02	1
9	160	12	0.02	0.02	1

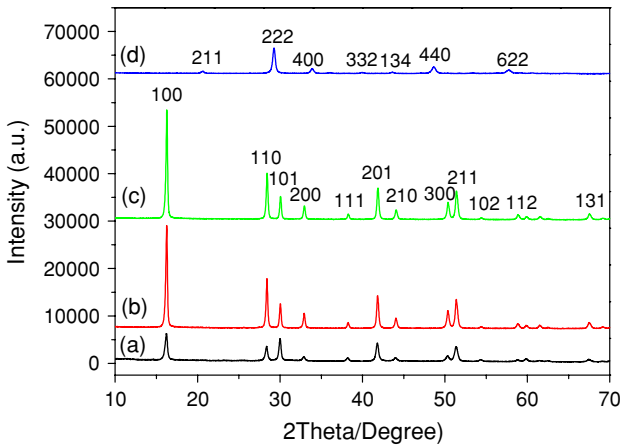

Fig. 1 XRD patterns of the product obtained after reaction for 12 h at (*a*) 80 °C (sample 8); (*b*) 160 °C (sample 9); (*c*) 200 °C (sample 1), and (*d*) after thermal decomposition of sample 1 at 700 °C for 4 h

found. An examination of the products showed that the microspindles have a length of about 6 μm and a diameter of about 1.2 μm in the middle part (Fig. 3a). Prolonging the reaction time to 6 h, the microspindles have a length of about 8 μm and a diameter of about 1.7 μm in the middle part (Fig. 3b). At this stage, most of the small particles disappear through an Ostwald ripening process and well crystallized and longer and larger nanorod nanobundles are obtained when the reaction time is increased to 12 h.

Effect of the concentration of EDTA

Here, we stress the important influence of the concentration of EDTA on the shape formation with other experimental conditions unchanged. Without the addition of EDTA, the synthesized $Y(OH)_3$ grows into microtubes with diameter in the range of 2–4 μm, and lengths range up to around 60 μm, which will be published elsewhere. When the EDTA concentration is 0.04 M, nanorod bundles have an average length of about 10.5 μm and a diameter of about 2.5 μm in the middle part are obtained (Fig. 4a), which is similar with the products obtained when the EDTA concentration is 0.02 M (Fig. 2a, b). Increasing the concentration of EDTA

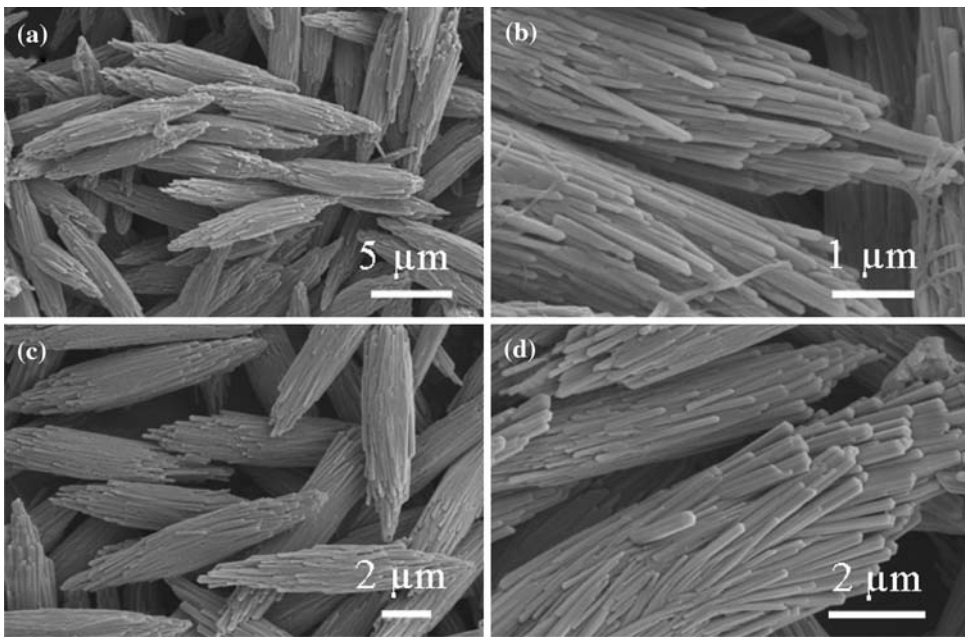

Fig. 2 SEM photos of the product. **a** and **b** sample 1; **c** and **d** after thermal treatment sample 1 at 700 °C for 4 h

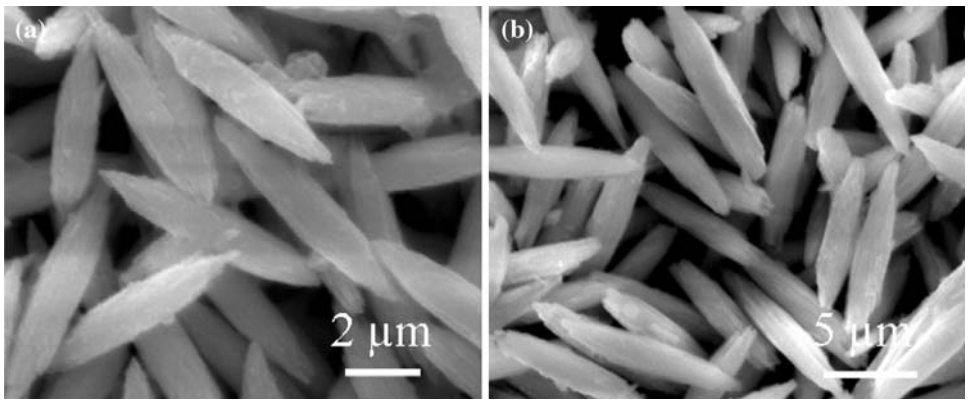

Fig. 3 SEM photos of the samples prepared at different growth stages. **a** 1 h (sample 2) and **b** 6 h (sample 3)

to 0.1 M, the products are not as uniform as the products obtained at low EDTA concentration. The nanorod bundles are in the lengths varying from 5 to 15 μm and diameters ranging from smaller than 2 μm to larger than 3 μm in the middle part. Furthermore, by fine observation, some of the nanorod bundles are not well formed (Fig. 4b). From above it can be seen that the addition of EDTA is essential for the formation of $Y(OH)_3$ nanorod bundles. As is well known, EDTA is an efficient chelator for rare earth ions. Its chelation constant ($\lg\beta 1$) for Y^{3+} is 18.09. The presence of EDTA is found to be helpful for the formation of several types of ultrafine particles. For example, Yi et al. study the role of the EDTA in the preparation of $NaYF_4$: Yb^{3+}/Er^{3+} spherical nanoparticles [24]. It is believed that the addition of EDTA plays two roles in the formation: (1) it forms stable $Y(EDTA)^-$ (1:1) complexes which bring about decrease both in the nucleation process and in nuclei growth; (2) it will be absorbed on the surface of the newly formed products and thus prevents particle coagulation by shielding the rare earth ions. In this case, on the one hand, EDTA forms stable $Y(EDTA)^-$ (1:1) complexes and the Y^{3+} ions are presumably in a concentration zone more favorable to produce $Y(OH)_3$ nanorods. On the other hand, the relaxed EDTA ions will be selectively absorbed on some crystallographic planes of the $Y(OH)_3$ nanorods, which is in favor of the self-assembly of the $Y(OH)_3$ nanorods into nanorod bundles.

Effect of the concentration of NaOH

The effect of the concentration of NaOH on the synthesis was also investigated. When the concentration of NaOH is 3 M, the products have an average length of about 6 μm and a diameter in the middle part of about 1 μm (Fig. 5a), which is shorter and slimmer than those of the products prepared when the concentration of NaOH is 1 M. Furthermore, the spindlelike structures are not well formed. Similar results were obtained when the concentration of NaOH is 5 M (Fig. 5b). The products are with an average length of about 10 μm and a diameter of about 1.4 μm in the middle part. Similarly, the nanorod bundles are also not well formed. From the experimental results, it seems that low concentration of NaOH is in favor of the formation of well formed nanorod bundles. It is well known that the pH value has great effect on the morphology and size of the final products. For example, the influence of pH value on the morphology of the $Sm(OH)_3$ has been investigated by Li et al. [2]. Their results show that there exists an optimal pH value for the growth of high-aspect-ratio nanowires. They think this phenomenon can be explained by the complex interaction and balance between the chemical potential and the rate of ionic motion. In this case, when the concentration of NaOH is low, high rate of ionic motion and low chemical potential environment were obtained. Maybe the solution environments are helpful for

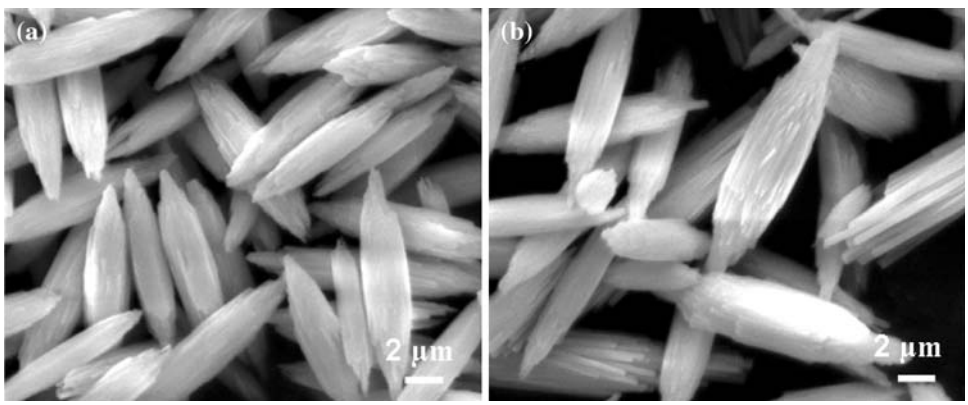

Fig. 4 SEM photos of the samples prepared with different concentration of EDTA. **a** 0.04 M (sample 4) and **b** 0.1 M (sample 5)

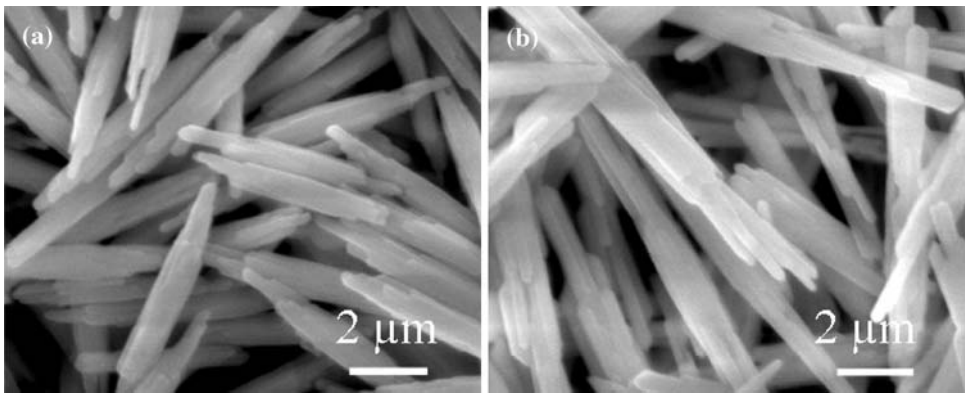

Fig. 5 SEM photos of the samples prepared at different concentration of NaOH. **a** 3 M (sample 6) and **b** 5 M (sample 7)

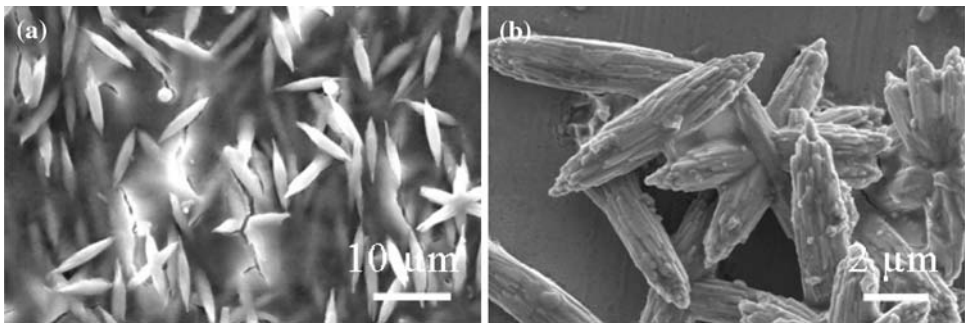

Fig. 6 SEM photos of samples prepared at different temperatures. **a** 80 °C (sample 8); **b** 160 °C (sample 9)

the self-assembling of the nanorods into well formed $Y(OH)_3$ nanorod nanobundles.

Effect of reaction temperature

To investigate the effect of reaction temperature on the synthesis, experiments were carried out at 80 and 160 °C, while the other experimental conditions were kept unchanged. Figure 6a shows the SEM image of the product obtained at 80 °C. The obtained $Y(OH)_3$ nanorod bundles have an average length of about 7 μm and a diameter of about 1.4 μm in the middle part. Moreover, many small particles smaller than 100 nm are found in the product which implying that the products are not well crystallized. Increasing the reaction temperature to 160 °C, nanorod bundles are the main products. Compared with the sample prepared at 80 °C, the nanorod bundles become longer and larger. The nanorod bundles have an average length of about 8 μm and a diameter of about 1.6 μm in the middle part. However, the microspindle is not well crystallized either, many small particles are also found on the surface of the nanorod bundles. Compared with the products prepared at 200 °C, it can be seen that the crystallinity of the product increases with the increase of the reaction temperature, which also can be verified by the XRD results.

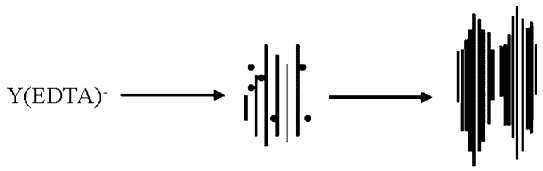

Fig. 7 Illustration for the formation of $Y(OH)_3$ microspindles under hydrothermal conditions

Formation mechanism for the $Y(OH)_3$ nanorod bundles

Based on above results, a mechanism for the formation of $Y(OH)_3$ nanorod bundles is suggested, as shown in Fig. 7. First, with the addition of EDTA, it can slow down the nucleation and subsequent crystal growth of the $Y(OH)_3$ particles, because EDTA forms strong complex with Y^{3+} through coordination interaction. With the addition of NaOH, it reacts with $Y(EDTA)^-$ to produce $Y(OH)_3$ nanoparticles and nanorods. At the same time, the dissociated EDTA ions enter into the solution again. The freshly formed nonorods self-assemble to form nanobundles with the assistance of EDTA ions, offering lower surface energy. During the reaction, the dissociated EDTA may act as a capping reagent to kinetically control the growth rate of different crystal faces through selective absorption and desorption. The length changes of the nanorod are probably

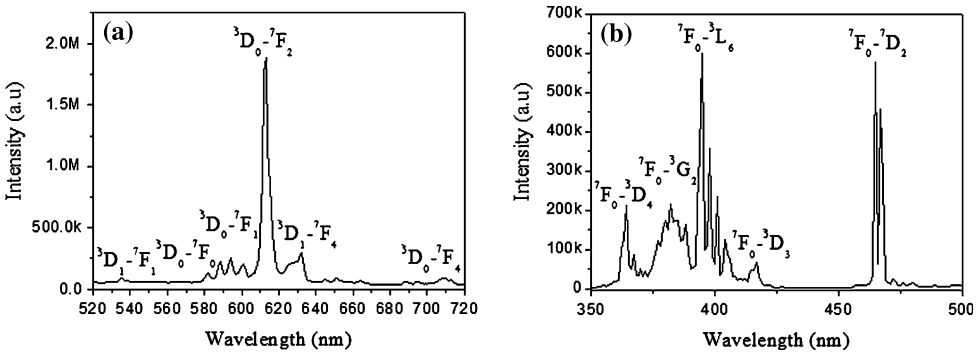

Fig. 8 **a** Emission and **b** excitation spectra of the as-prepared Y_2O_3:Eu^{3+} (5%) nanorod bundles

due to differences in the chemical potential of the rod ends versus the solution and it is the nucleation delays which are responsible for the length differences with the surrounding rods compared to the core nanorod which was the initial one. During the formation, the formed nanoparticles consume through an Ostwald ripening process because of curvature radius differences between them and nanorods parts (the ends probably). Finally, $Y(OH)_3$ nanorod bundles which are composed of nanorods are obtained.

Photoluminescence properties of the Y_2O_3:Eu^{3+} nanorod bundles

The Y_2O_3:Eu^{3+} nanorod bundles exhibit a strong red emission under under 393 nm excitation, and the spectral properties are typical of the well-known Y_2O_3:Eu^{3+} [25], as shown in Fig. 8. The emission spectrum is composed of $^5D_0 \rightarrow {}^7F_J$ transitions ($J = 0$, 1, 2, 3, and 4), with $^5D_0 \rightarrow {}^7F_2$ (613 nm) transition being the most prominent group (Fig. 8a). All the other peaks at 582, 594, 632, and 709 nm can be assigned to the $^5D_0$–$^7F_0$, $^5D_0$–$^7F_1$, $^5D_1$–$^7F_4$, and $^5D_0$–$^7F_4$ transitions, respectively. The corresponding emission peaks at 535 nm are attributed to the $^5D_1$–$^7F_1$. The strongest peak at 613 nm indicates that Eu^{3+} occupies a site without an inverse center in Y_2O_3 matrix. Figure 8b presents the room-temperature excitation spectrum of Y_2O_3:Eu^{3+} nanorod bundles, which shows the double excitation peaks at 393 and 465 nm, and the strongest peak is at 393 nm, so we select it as the excited light.

Conclusion

In summary, spindlelike $Y(OH)_3$ nanorod bundles composed of numerous nanorods have been synthesized via a facile hydrothermal method with the presence of EDTA. The effects of the reaction temperature, reaction time, and the concentration of EDTA and NaOH have been investigated. Results show that EDTA acting as shape modifier for the formation of spindlelike nanorod bundles. It can modulate the growth rate of different crystallographic facets to govern the final morphology. Y_2O_3:Eu^{3+} with similar morphology was obtained after thermal treatment of the $Y(OH)_3$:Eu^{3+} nanorod bundles at 700 °C for 4 h. A possible mechanism for the formation of $Y(OH)_3$ nanorod bundles is briefly suggested. Strong red emission centering at 613 nm is realized in the Eu^{3+} doped Y_2O_3 nanorod bundles which may find potential application in the field of color display and solid-state lasers.

Acknowledgements S. L. Zhong acknowledges the funding support from Projects under Scientific and Technological Planning of Education Office of Jiangxi Province.

References

1. Adachi GY, Imanaka N (1998) Chem Rev 98:1479
2. Wang X, Li YD (2002) Angew Chem Int Ed 41:4790
3. Hasegawa Y, Thongchant S, Wada Y, Tanaka H, Kawai T, Sakata T, Mori H, Yanagida S (2002) Angew Chem Int Ed 41:2073
4. Kim BN, Hiraga K, Morita K, Sakka Y (2001) Nature 413:288
5. Rosenflanz A, Frey M, Endres B, Anderson T, Richards E, Schardt C (2004) Nature 430:761
6. Lin TS, Sobotka LG, Froncisz W (1988) Nature 33:321
7. Edwin Suresh Raj AM, Maria Magdalane C, Nagaraja KS (2002) Phys Status Solid A 191:230
8. Nomura K, Ohta H, Takagi A, Kamiya T, Hirano M, Hosono H (2004) Nature 432:488
9. Silver J, Martinez-Rubio MI, Ireland TG, Fern GR, Withnall R (2001) J Phys Chem B 105:948
10. Bolchouchine VA, Goldburt ET, Levonovitch BN, Litchmanova VN, Sochtine NP (2000) J Lumin 87–89:1277
11. Wang X, Sun XM, Yu DP, Zou BS, Li YD (2003) Adv Mater 15:1442
12. Fang YP, Xu AW, You LP, Song RQ, Yu JC, Zhang HX, Li Q, Liu HQ (2003) Adv Funct Mater 13:955
13. Li W, Wang X, Li Y (2004) Chem Commun 2:164
14. Wu XC, Tao YR, Gao F, Dong L, Hu Z (2005) J Cryst Growth 277:643
15. Li Q, Feng C, Jiao Q, Guo L, Liu C, Xu HB (2004) Phys Status Solidi A 201:3055
16. Xue B, Song HW, Yu LX, Yang LM, Liu ZX, Pan GH, Lu SZ, Ren XG, Lei YH, Fan LB (2005) J Phys Chem B 109:15236
17. Wan JX, Wang ZH, Chen XY, Mu L, Qian YT (2005) J Cryst Growth 284:538

18. Xu ZX, Hong ZL, Zhao QC, Peng LX, Zhang PY (2006) J Rare Earths 24:111
19. Han M, Shi NE, Zhang WL, Li BJ, Sun JH, Chen KJ, Zhu JM, Wang X, Xu Z (2008) Eur Chem J 14:1615
20. He Y, Tian Y, Zhu Y (2003) Chem Lett 32:862
21. Si R, Zhang YW, You LP, Yan CH (2005) Angew Chem Int Ed 44:3256
22. Zhang J, Liu ZG, Lin J, Fang JY (2005) Cryst Growth Des 5:1527
23. Hu CQ, Gao ZH (2006) J Mater Sci 41:6126. doi:10.1007/s10853-006-0450-8
24. Yi GS, Lu HC, Zhao SY, Yue G, Wang WJ, Chen DP, Guo LH (2004) Nano Lett 4:2191
25. Yang J, Quan ZW, Kong DY, Liu XM, Lin J (2007) Cryst Growth Des 7:730